# Biphasic co-flow through a sudden expansion or contraction of a Hele-Shaw channel

Boris Y. Rubinstein [1], Dana Zusmanovich [2], Zhenzhen Li,[3] and Alexander M. Leshansky [2,*]

[1]*Stowers Institute for Medical Research, 1000 E 50th Street, Kansas City, Missouri 64110, USA*
[2]*Department of Chemical Engineering, Technion, Haifa 32000, Israel*
[3]*School of Aerospace Engineering, Beijing Institute of Technology, Beijing 100081, China*

In the present paper we study the biphasic co-flow through a Hele-Shaw cell with an abrupt change, either expansion or contraction, in channel width. Assuming gentle variation of the flow in the streamwise direction (valid at small capillary number), we derive the third-order nonlinear differential equation governing the shape of the interface separating the two fluids. The interfacial profiles obtained by solving this nonlinear equation are further used as the initial guess for the interface shape in the rigorous numerical solution of the two-dimensional free-boundary problem by the finite element method. The theoretical results are then compared with the experimental findings showing a good agreement. The amplitude of the capillary ridge emerging upstream from a sudden expansion (for moderate expansion ratios up to 1:3) and leading to narrowing of the thread of the disperse phase is significant, however not large enough to trigger its instability and breakup.

## I. INTRODUCTION

The so-called Hele-Shaw flow [1] in which two immiscible fluids are confined to the thin gap between two parallel flat plates has a long history. The confinement is narrow, so that the vertical component of the velocity may be neglected, while the plates exert friction upon the fluids so that their depth-averaged two-component velocity along the plates may be described by a potential flow, mimicking the Darcy flow through a porous medium [2]. In their pioneering works Saffman and Taylor applied the Hele-Shaw formulation to model displacement of viscous fluid by a less viscous fluid [3] (known as the Saffman-Taylor problem) and determine the velocity and shape of a gas bubble [4] in a porous medium. While most later studies of the Saffman-Taylor type of problems (see [5]) employed the two-dimensional (2D) Hele-Shaw flow approximation, the realistic modeling of the dynamics of strongly confined (pancake-shaped) bubbles (or droplets) requires going beyond the 2D hydrodynamics by considering the 3D thin lubrication films sandwiched between the pancake droplet and the plates [6]. Thickness and topography of such films are dynamically controlled and should thus be determined as part of the solution, while the need for high spatial resolution within ultrathin lubrication films and small integration time step (both due to typically rather low capillary number) renders this problem computationally expensive [7,8].

Confined Hele-Shaw flows are particularly useful in droplet-based microfluidics. Hele-Shaw cells were exploited, for instance, to study dynamics of confined 2D droplet emulsions [9]; geometry-mediated breakup of biphasic and triphasic Hele-Shaw co-flow at the topological step (i.e., due to a sudden change in channel depth) is used for step emulsification, allowing for high-throughout production of highly monodisperse single [10–12] and double emulsions [13],

---

*lisha@technion.ac.il

respectively; vertically confined slug drops formed at the Hele-Shaw microfluidic T junction can be controllably broken into a collection of $N$ identical microdrops to be assembled into predesigned colloidal structures [14].

Stone and co-workers [15] demonstrated how the capillary instability of the biphasic co-flow in a Hele-Shaw geometry can be passively controlled by the channel geometry (i.e., its width $w$ or height $b$). The constant width $\ell$ of the thread of the disperse (inner) fluid 1, engulfed by the co-flowing continuous fluid 2, is given by $\ell/w = (1 + k)^{-1}$, where $k = q_2 \mu_2 / q_1 \mu_1$, with $q_i$ and $\mu_i$ being the flow rate and viscosity of the respective phase. For stable biphasic co-flow, the channel walls should be well wetted by the continuous fluid and poorly wetted by the disperse phase. Once the thread width becomes comparable to the channel height, $\ell \approx b$, the vertical confinement is lost and capillary (Rayleigh-Plateau) instability of a cylindrical liquid thread becomes operative resulting in its breakup into droplets. As long as the thread is well confined vertically, i.e., $\ell > b$, the capillary instability is suppressed and steady parallel co-flow takes place. This allows simple geometric control over the thread stability: a sudden change in the channel width $w$ or depth $b$ can either stabilize or destabilize the biphasic co-flow. These arguments, however, are only valid with regard to a steady parallel co-flow, while the flow and the shape of the thread in the vicinity of an abrupt transition in the channel geometry have not been previously investigated.

In Ref. [12] the shape of biphasic co-flow in a Hele-Shaw channel prior to the topological step, i.e., the inlet to a deep (and wide) reservoir, was studied. The confined thread of the inner liquid undergoes *capillary focusing* before the step due to loss of confinement and corresponding reduction in the capillary pressure and its shape can be described using the 2D Hele-Shaw hydrodynamics [12]. The shape of the thread was determined employing the long-wave approximation (assuming gentle variation of the flow in the streamwise direction, i.e., neglecting pressure variation across the channel) in Ref. [12], while this limitation was relaxed and the thread shape was computed numerically using the volume-of-fluid (VoF) formulation in Ref. [16]. Most recently, a similar problem of capillary focusing in triphasic co-flow in the Hele-Shaw channel was studied employing the finite element method (FEM) [13]. In these studies, however, the complex 3D flow in the reservoir beyond the step was not resolved, and some *ad hoc* outlet pressure boundary conditions had been imposed at the entrance to the reservoir.

In this paper we report a study of the biphasic co-flow through a Hele-Shaw channel with an abrupt (steplike) change of its *width* (i.e., expansion or contraction) that combines theory, experiments, and numerical solution, and determine the flow and the shape of the thread of the disperse (inner) fluid. In contrast to a biphasic flow through a Hele-Shaw channel conjugated with a deep reservoir, in this case the flow remains vertically confined meaning that the same Hele-Shaw formulation applies everywhere, i.e., upstream and downstream from the transition. We first derive the third-order nonlinear ordinary differential equation (ODE) that governs the shape of the free interface separating the two phases using the long-wave theory in Sec. II and then use this approximate solution as the initial guess for the numerical FEM scheme in Sec. III. The experimental setup is briefly described in Sec. IV, while the theoretical findings are compared with the experimental results in Sec. V.

## II. LONG-WAVE THEORY

Let us start with the description of the steady-state position of the free interface between the two immiscible co-flowing fluids. The micrographs of the biphasic co-flow through a Hele-Shaw cell with a sudden contraction and expansion are shown in Figs. 1(a) and 1(b), respectively. The depth-averaged velocity in the two immiscible fluid phases, i.e., inner (disperse) phase 1 and outer (continuous) phase 2, are governed by the quasi-2D Hele-Shaw equations (see, e.g., [2]):

$$\boldsymbol{v}_i = -\frac{b^2}{12\mu_i}\boldsymbol{\nabla}_\| p_i, \tag{1}$$
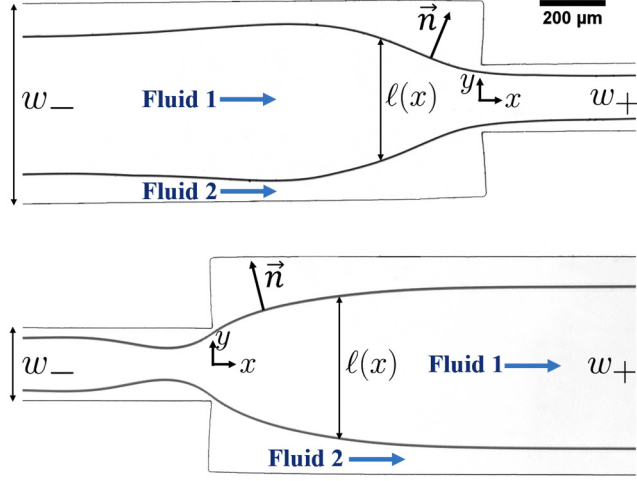
FIG. 1. Experimental micrographs of the biphasic Hele-Shaw flow through a sudden 3:1 contraction (upper panel) and 1:3 expansion (lower panel). The widths of the inlet and outlet channels are $w_{\pm}$, the local width of the inner fluid stream is $\ell(x)$; away from the expansion there is parallel co-flow with constant widths controlled by the flow rates and viscosities of the two phases (1: inner fluid; 2: outer fluid).

in which $p_i(x, y)$ is the pressure in the region occupied by $i$th fluid phase of viscosity $\mu_i$, $b$ is the cell height, and $\nabla_{\parallel} = \frac{\partial}{\partial x}\widehat{x} + \frac{\partial}{\partial y}\widehat{y}$ is the projection of the gradient operator onto the $(x, y)$ plane. We assume that the inner (e.g., organic) phase does not wet the channel walls, while the continuous (e.g., aqueous) phase perfectly wets the walls of the channel [the polydimethylsiloxane (PDMS) channel pretreated with plasma to render them hydrophilic; see Sec. IV for details]. We also assume that variations of the flow in the streamwise direction are gentle (the validity of the assumption will be discussed later) and the pressure variation *across* the channel is negligible. Rewriting the Hele-Shaw equations (1) via respective flow rates $q_i$ of the two fluids, we readily obtain

$$q_1 = -\frac{b^3 \ell}{12\mu_1}\frac{dp_1}{dx}, \quad q_2 = -\frac{b^3(w_{\pm} - \ell)}{12\mu_2}\frac{dp_2}{dx}, \tag{2}$$

where $w_-$ and $w_+$ are the respective widths of the inlet (left) and outlet (right) Hele-Shaw cells satisfying $w_{\pm} \gg b$, and $\ell(x)$ is the local stream width (of the inner fluid 1) in both channels.

At the stationary interface separating the two co-flowing phases in a Hele-Shaw cell, the pressure jump is balanced by the Laplace (capillary) pressure due to a constant transverse curvature of semicircular menisci of radius $b/2$ and the varying 2D curvature (with radius of curvature $\mathcal{R} \gg b$) of the projection of the tip of the meniscus, $y = \pm\ell(x)/2$, onto the horizonal $(x, y)$ plane (see the Appendix for details),

$$p_1 - p_2 \approx \gamma\left(\frac{2}{b} + \frac{\pi}{4}\nabla_{\parallel}\cdot\boldsymbol{n}\right) \approx \gamma\left(\frac{2}{b} - \frac{\pi}{4}\ell_{xx}\right), \tag{3}$$

where $\gamma$ is the surface tension, $\boldsymbol{n}$ is the unit normal to the projection of the tip of the meniscus in $(x, y)$ plane (pointing into the continuous phase 2; see Fig. 1); the last approximate equality holds assuming gentle variance in the streamwise direction, i.e., $\ell_x^2 \ll 1$. The boundary condition (3) is in agreement with a more general condition for the pressure jump across the *moving* (along $\boldsymbol{n}$) boundary in a problem of two-phase displacement in a Hele-Shaw cell [17]. Notice that the dynamical contribution to the pressure jump in [17] (reported earlier by [18]), $\propto \mathcal{O}(\frac{\gamma}{b}\mathrm{Ca}_n^{2/3})$ to the leading approximation, where the capillary number $\mathrm{Ca}_n = U_n\mu_2/\gamma$ is based on the velocity of the interface displacement $U_n$, vanishes in the present case, since $U_n = 0$. It is also worth mentioning

that in contrast to the problem of two-phase displacement in [17], where the vertical thickness of the film of the continuous fluid 1 sandwiched between the bounding horizontal walls of the cell and the disperse phase is determined *dynamically*, in the present problem it should be determined from static considerations (balance between, e.g., van der Waals, electrostatic, or other forces).

Differentiating the last equation with respect to $x$, substituting the pressure gradients from (2), and introducing dimensionless variables $\eta = \ell/w_-$, $\zeta = x/w_-$, we arrive at the single nonlinear ODE for the scaled width of the thread:

$$\epsilon^{-1} \, \eta_{\zeta\zeta} = \frac{1}{\eta} - \frac{k}{\alpha - \eta}, \tag{4}$$

where $k = \mu_2 q_2 / \mu_1 q_1$, $\epsilon = \mathrm{Ca}\beta^2$ with the capillary number being defined as $\mathrm{Ca} = 48\mu_1 q_1 / \pi \gamma b w_-$ and $\beta = w_-/b \gg 1$ is the aspect ratio of the inlet Hele-Shaw channel. Here $\alpha$ is the Heaviside step function:

$$\alpha = \begin{cases} 1, & \zeta < 0, \\ A, & \zeta \geqslant 0, \end{cases}$$

where the width ratio $A = w_+/w_- > 1$ or $A < 1$ for expansion and contraction, respectively. Since the height of channel is fixed, we expect the interface to be a smooth function of the position so that Eq. (4) holds everywhere and there is no need for matching the separate solutions obtained in the inlet and outlet channels at their conjugation at $\zeta = 0$.

Notice that the flow is governed by the parameter $\epsilon$ (modified capillary number), which is equal to Ca multiplied by a large factor of the (inlet) cell aspect ratio squared, $\beta = (w_-/b)^2 \gg 1$, emphasizing the importance of the viscous forces (due to large transverse velocity gradients) in a strongly confined Hele-Shaw geometry. In other words, in a Hele-Shaw cell the flow dominated by the surface tension requires not just $\mathrm{Ca} \ll 1$, but a more restrictive condition, $\mathrm{Ca} \ll (b/w_-)^2 \ll 1$. It can be readily seen from (4) that $\ell_x = \mathcal{O}(\epsilon^{\frac{1}{3}})$ and, therefore, the assumption of gentle variations in the flow direction requires $\epsilon^{\frac{1}{3}} = o(1)$, similarly to the well-known thin film lubrication equation (e.g., [18]). However, in most practical cases [10–12] $\epsilon = \mathcal{O}(1)$ or higher due to the large factor of $(w_-/b)^2$ multiplying small Ca. For now we shall assume that the long-wave approximation holds and address its accuracy later on by comparing its prediction to the rigorous FEM numerical solution.

One can also eliminate the parameter $\epsilon$ containing Ca in (4) by rescaling the streamwise coordinate, $\xi = \epsilon^{\frac{1}{3}}\zeta$. In terms of $\xi$ the Eq. (4) becomes

$$\eta''' = \frac{1}{\eta} - \frac{k}{\alpha - \eta}, \tag{5}$$

where the prime stands for $d/d\xi$. Notice that the rescaled Eq. (5) does not contain Ca, while the rescaled distance $\xi \propto \mathrm{Ca}^{\frac{1}{3}}$ is a weak function of Ca, indicating that the resulting interfacial profiles do not strongly vary with the capillary number. Far upstream or downstream from the expansion (or contraction) at $\xi \to \pm\infty$, we have $\eta_{\xi\xi\xi} \to 0$ and $\eta \to \eta_{\pm\infty}$, whereas from (5) one can readily find the simple closed-form solution for the parallel co-flow far from $\xi = 0$:

$$\eta_{\pm\infty} = \frac{\ell_{\pm\infty}}{w_-} = \frac{\alpha}{1 + k}. \tag{6}$$

The validity of Eq. (6) was demonstrated experimentally in [15], justifying the applicability of the quasi-2D Hele-Shaw equations (2) in the presence of thin lubricating films of the continuous phase separating the confined thread and the walls of the channel.

At some finite distance upstream or downstream from the expansion (or contraction) at $\xi = 0$, the stream width $\eta(\xi)$ starts to slightly deviate from the constant width $\eta_{\pm\infty}$ in Eq. (6), so we can write $\eta = \eta_{\pm\infty} + \widetilde{\eta}$, where $|\widetilde{\eta}| \ll |\eta_{\pm\infty}|$. When $\eta$ is close to $\eta_\infty$, the Eq. (5) can be linearized:

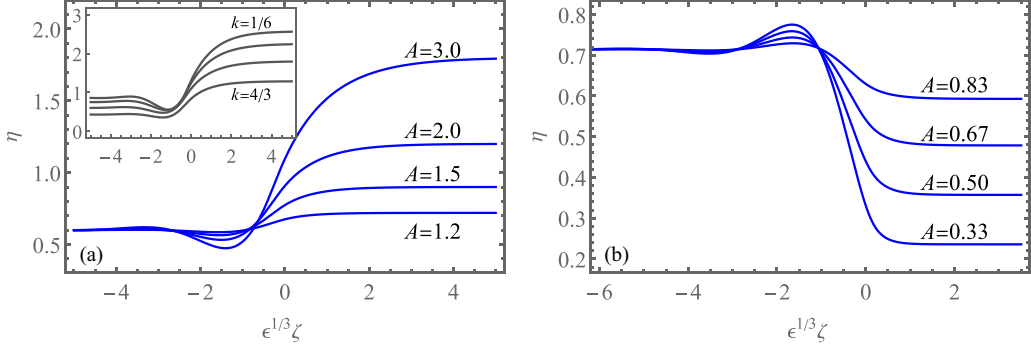$$\widetilde{\eta}''' + \lambda^3 \widetilde{\eta} = 0 \, , \tag{7}$$

FIG. 2. The inner stream width $\eta$ vs the rescaled axial distance $\xi = \epsilon^{\frac{1}{3}}\zeta$ computed using the long-wave approximation: (a) sudden expansion for fixed value of $k = 2/3$ upon varying the width ratio $A = w_+/w_- = 1.2, 1.5, 2,$ and 3. The inset shows the same for an expansion with fixed width ratio $A = 3$ for $k = 1/6, 1/3, 2/3,$ and $4/3$; (b) sudden contraction for a fixed value of $k = 0.4$ upon varying the width ratio $A = 0.33, 0.5, 0.67,$ and $0.83$.

where $\lambda = (1 + k)/(\alpha^2 k)^{\frac{1}{3}}$. The linearized Eq. (7) can be readily solved to give

$$\widetilde{\eta} = ae^{-\lambda\xi} + be^{\frac{1}{2}\lambda\xi}\cos\left(\frac{\sqrt{3}}{2}\lambda\xi\right) + ce^{\frac{1}{2}\lambda\xi}\sin\left(\frac{\sqrt{3}}{2}\lambda\xi\right),$$

where $a$, $b$, and $c$ are integration constants. As $\widetilde{\eta}$ should decay away from the expansion we can explicitly write the asymptotic form of the solution upstream at $\xi \to -\infty$:

$$\eta \approx \frac{1}{1 + k} + be^{\frac{1}{2}\lambda_-\xi}\cos\left(\frac{\sqrt{3}}{2}\lambda_-\xi\right) + ce^{\frac{1}{2}\lambda_-\xi}\sin\left(\frac{\sqrt{3}}{2}\lambda_-\xi\right),$$

where $\lambda_- = (1 + k)/k^{\frac{1}{3}}$, and downstream at $\xi \to \infty$

$$\eta \approx \frac{A}{1 + k} + ae^{-\lambda_+\xi}, \tag{8}$$

where $\lambda_+ = (1 + k)/(A^2 k)^{\frac{1}{3}}$.

These asymptotic results indicate the appearance of the capillary wave (ridge) with an amplitude decaying exponentially fast upstream from the transition as $\xi \to -\infty$. A similar capillary ridge emerges at the rear end of Bretherton's slender bubble moving in a tube [18] and in free unbounded [19,20] and confined [21] viscous films flowing over topography. An interesting question is whether the emergence of the capillary ridge may destabilize the thread at the expansion (contraction), even though its width far upstream or the downstream width satisfies $\ell_{\pm\infty} \gg b$.

We solve the two-point boundary value problem in Eqs. (5) and (6) as the initial value problem using the "shooting" method. We numerically integrate Eq. (5) starting from some large value of $\xi = \xi_p$ upstream in the negative $\xi$ direction to some large (negative) value of $\xi = -\xi_m$, where the parallel co-flow takes place. We use the asymptotic form of the solution upstream (8) to determine the value of the function and its two derivatives at $\xi = \xi_p$: $\eta' = -a\lambda_+ e^{-\lambda_+\xi_p}$ and $\eta'' = a\lambda_+^2 e^{-\lambda_+\xi_p}$. The adjustable constant $a$ is varied to satisfy the downstream boundary condition at $\xi = -\xi_m$ of the parallel co-flow, i.e., $\eta \approx 1/(1 + k)$.

The obtained results for the thread width are shown in Figs. 2(a) and 2(b) for expansion and contraction, respectively, vs the rescaled streamwise distance $\epsilon^{\frac{1}{3}}\zeta$ upon varying the width ratio $A$ for a fixed upstream thread width (for $k = 2/3$). It can be observed that prior to a transition (at $\xi = 0$) there is a capillary ridge of magnitude that enhances with the increase in expansion ratio $A$ (or $A^{-1}$ for contraction). The inset in Fig. 2(a) shows the stream width in a sudden 1:3 expansion

upon varying $k$ (the constant upstream width of the thread $\eta_{-\infty}$). Notice that the amplitude of the capillary ridge increases slowly as $k$ decreases, reaching $\approx 60\%$ of $\eta_{-\infty}$ in Eq. (6) for $k = 1/6$, meaning that sudden 1:3 expansion cannot trigger capillary instability and perhaps transition to a much wider outlet channel is needed in order to destabilize the thread. This conclusion, of course, relies on the accuracy of the long-wave approximation which we shall test below.

## III. NUMERICAL SCHEME

We use the finite element method (FEM) package in *Mathematica* [22] to solve the problem for pressure, $p_i(x, y)$, numerically. The simulation domain is the upper half of the two conjugated Hele-Shaw channels (due to reflection symmetry at $y = 0$), $[(-L_m, 0), (0, 1/2)] \cup [(0, L_p), (0, A/2)]$, where all lengths are scaled with the width of the inlet channel, $w_-$: $\zeta = x/w_-$, $\eta = y/w_-$.

The pressure in both phases is normalized with $p_* = 12\mu_1 q_1/b^3$ and it is a harmonic function satisfying the Laplace equation, i.e., $\hat{\nabla}^2 \hat{p}_i = 0$ ($i = 1, 2$). At the side walls the conditions are the zero flux, i.e., either $\partial \hat{p}_i/\partial \zeta = 0$ or $\partial \hat{p}_i/\partial \eta = 0$, depending on the boundary, including at the centerline ($\eta = 0$) due to symmetry. The inner phase 1 at the left boundary (at $\zeta = -L_m$) occupies the interval $0 < \eta < \frac{1}{2}(1 + k)^{-1}$, while the outer phase 2 occupies the interval $\frac{1}{2}(1 + k)^{-1} < \eta < \frac{1}{2}$. Similarly, at the outlet (at $\zeta = L_p$) the inner phase 1 occupies the interval $0 < \eta < \frac{1}{2}A(1 + k)^{-1}$, and the phase 2 occupies the interval $\frac{1}{2}A(1 + k)^{-1} < \eta < \frac{1}{2}$. Within the domain the two fluids are separated by the free boundary $\eta = \hat{f}(\zeta)$ whose position has to be found.

At the left (inlet) boundary the pressure derivatives are determined by the constant flow rates of both phases:

$$\frac{\partial \hat{p}_1}{\partial \zeta} = \frac{\partial \hat{p}_2}{\partial \zeta} = -(1 + k), \quad \frac{\partial \hat{p}_{1,2}}{\partial \eta} = 0 \quad \text{at} \ \zeta = -L_m. \tag{9}$$

At the right (outlet) boundary the pressure difference across the interface (assuming parallel co-flow) is just $p_1 - p_2 = 2\gamma/b$, and then in the dimensionless form it gives the following (outlet pressure) conditions:

$$\hat{p}_1 = \frac{8}{\pi}\epsilon^{-1}\beta, \quad \hat{p}_2 = 0 \quad \text{at} \ \zeta = L_p, \tag{10}$$

where we recall that $\epsilon = \text{Ca}\beta^2$ with the capillary number being defined as $\text{Ca} = 48\mu_1 q_1/\pi\gamma bw_-$ and $\beta = w_-/b \gg 1$ being the inlet channel aspect ratio. The kinematic condition at the free boundary, $\eta = \hat{f}(\zeta)$, separating the two immiscible phases at steady state, is $\partial \hat{p}_i/\partial n = 0$. The normal stress (pressure jump) boundary condition in Eq. (3) rewritten in the dimensionless form reads

$$\hat{p}_1 - \hat{p}_2 = \epsilon^{-1}\left(\frac{8}{\pi}\beta + \widehat{\nabla}_\parallel \cdot \boldsymbol{n}\right) \quad \text{at} \ \eta = \hat{f}(\zeta), \tag{11}$$

where the in-plane mean curvature is computed as $\widehat{\nabla}_\parallel \cdot \boldsymbol{n} = -\hat{f}''/(1 + \hat{f}'^2)^{3/2}$.

We use the long-wave approximation, $\hat{f}(\zeta) = \frac{1}{2}\eta(\epsilon^{\frac{1}{3}}\zeta)$, as the initial guess for the position of the free boundary. The Laplace equation for the harmonic pressure is solved using FEM in each of the domains occupied by the two phases subject to the conditions $\partial \hat{p}_{1,2}/\partial n = 0$ at the free interface and the corresponding inlet and outlet boundary conditions (9) and (10). Then the interface is discretized and the pressure difference, $\hat{p}_1 - \hat{p}_2$, across the interface is computed at each point. Then the interface position is shifted in the direction of the local normal $\vec{n}$ in order to minimize the difference between the actual and the prescribed in (11) pressure jump.

The boundary is defined as a discrete set of equidistant points which is used to produce a smooth boundary employing third-order interpolation. After the position of the boundary is updated, a new interpolation via the updated set of points is performed to maintain interface smoothness. The Laplace equation for the pressure $\hat{p}_i$ is then solved again in the updated domains 1 and 2 and the procedure is repeated until convergence, i.e., until pressure difference in (11) is satisfied

within a prescribed accuracy of $5 \times 10^{-4}$ everywhere. Notice that due to the Neumann condition at the free boundary for the pressure, shifting the free interface along the local normal results in the second-order accuracy numerical scheme.

## IV. EXPERIMENTAL SETUP

### A. Microfluidic device

The device is made of PDMS replicated from a silicon wafer, which is fabricated via standard photolithography. The channel has two inlets, one for the inner (oil) phase, the other for the outer (aqueous) phase. The two fluid phases are injected separately, meet at a junction, and co-flow through a shallow Hele-Shaw channel. The outer aqueous phase wets the walls of the channels and it completely engulfs the oil stream. The Hele-Shaw channel has the height $b = 20$ $\mu$m and different widths of the inlet channel: $w_- = 200$, 400, and 600 $\mu$m corresponding to the channel aspect ratio $\beta = w_-/b = 10$, 20, and 30, respectively. The fluids co-flow through an abrupt change of channel width $w_- \to w_+$, with the channel width ratio $A = w_+/w_- = 1.5$, 2, 3 (for expansion) and $A = 0.67$, 0.5, and 0.33 (for contraction). The two fluids are injected into the microchannel by syringe pumps (Longerpump LSP02-2A) with glass syringes (Hamilton 500 $\mu$l and 1 ml) allowing for tight control over the values of the parameters Ca and $k$. The flow is monitored through a microscope (Nikon Ti2-U), and microphotographs are taken using a fast camera (Photron Fastcam SA5).

### B. Microfabrication

Geometry of the microchannels is designed by AutoCAD (Autodesk, USA), a silicon wafer is fabricated with a standard photolithography [11,12]. The channel is fabricated from polydimethylsiloxane (PDMS) by mixing the resin with a curing agent (Sylgard 184, Dow Corning) at weight ratio 9:1. The mixture is then centrifuged to eliminate air bubbles prior to being poured onto the silicon wafer with channel layout. The entity is heated in an oven at 85 °C for 1.5 h. Then the PDMS block is peeled off from the silicon wafer. Holes for connecting the tubes are punched at the inlets and outlets of the PDMS channel. The glass slide is glued onto the PDMS block using plasma cleaner (Harrick Plasma PDC-32G-2) to form a sealed channel. The channel is rendered hydrophilic following the plasma treatment, and hydrophilicity can be maintained for an extended period of time provided that the aqueous solution is injected into the channel immediately right after the plasma treatment [13].

### C. Fluid characterization

A fluorinated oil FC40 (3M, USA) is used as the inner phase, and an aqueous glycerol solution at concentration (40% w/w) is used as the continuous (outer) phase. The surface tension between the two fluids is 45.3 mN/m measured by the pendent drop method (Dataphysics, OCA20). The viscosity of FC40 oil is 4.2 mPa s, and that of the glycerol solution is 3.72 mPa s, both measured by a cone-and-plate rheometer (Anton-Paar MCR 302, with a rotor CP50-1 with 50 mm diameter and a cone angle of $1°$) at the temperature of $20$ °C.

## V. RESULTS AND DISCUSSION

The approximate theory in Sec. II suggests that the biphasic co-flow through a sudden expansion (or contraction) is only weakly dependent on the capillary number, via Ca$^{\frac{1}{3}}$ dependence of the rescaled axial distance $\xi$. Figure 3 depicts the experimentally measured stream width of the disperse phase 1 (symbols) in a sudden 2:1 contraction obtained upon proportionally varying the flow rates of both phases, such that $q_2/q_1 = $ const. Under these conditions Ca is varied, while $k$ is kept constant. Inspired by the scaling of the approximate solution, we plot the experimental results vs the rescaled axial distance $\epsilon^{\frac{1}{3}}\zeta$. It can be readily seen that the result is independent of the capillary number, as all
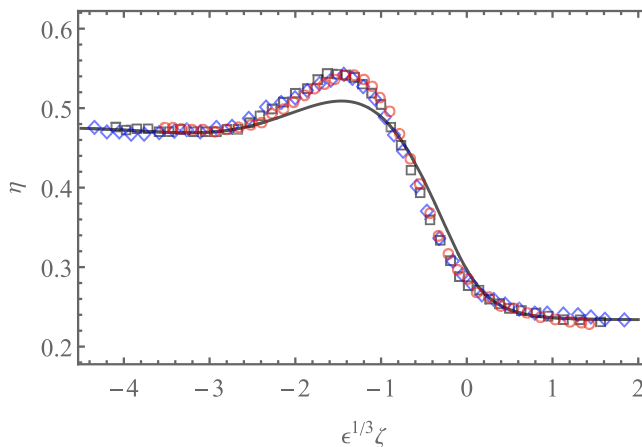
FIG. 3. The experimentally measured width of the thread of the disperse phase $\eta$ plotted vs the rescaled axial distance $\xi = \epsilon^{\frac{1}{3}}\zeta$ for a sudden 2:1 contraction for $\beta = 20$ and fixed value of $k = 1.12$ upon varying the capillary number: $Ca = 0.0039$ ($\circ$), $0.0058$ ($\square$), and $0.0078$ ($\diamond$). The solid curve stands for the long-wave approximate solution.

points corresponding to different Ca's fall on the same master curve. The long-wave solution (solid line) does not approximate the master curve closely everywhere (in particular the magnitude of the capillary ridge before the contraction is somewhat underestimated by the theory), since contrary to the assumption of the theory, in the experiment $\epsilon$ is not small and varies between 1.6 and 3.2.

The comparison between the experimental profiles (symbols) and the numerical prediction (solid lines) are depicted, using equal aspect ratio of both axes, in Figs. 4(a)–4(d) for some selected values of $A$. The long-wave approximate profiles (shown for comparison as dashed lines), were used in the numerical solution as the initial guess for the interface position. In all cases the agreement between the numerical and experimental results is rather close, although not excellent; the numerical solution
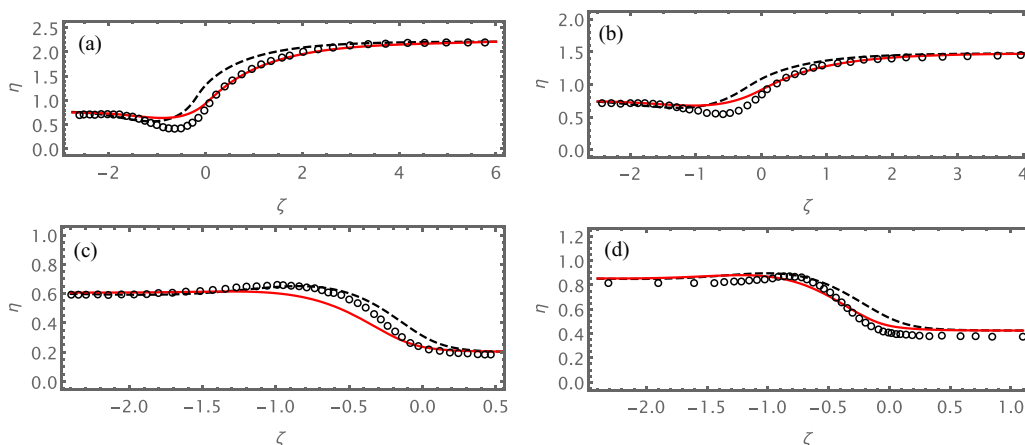


FIG. 4. The width of the inner fluid thread $\eta$ vs dimensionless axial distance $\zeta$: the experimental results (empty circles), the numerical prediction (red solid lines), and the long-wave approximation (dashed lines). (a) 1:3 expansion with $k = 0.354$, $Ca = 0.0148$, and $\beta = 10$ ($\epsilon = 1.48$); (b) 1:2 expansion with $k = 0.354$, $Ca = 0.0148$, and $\beta = 10$ ($\epsilon = 1.48$); (c) 3:1 contraction with $k = 0.664$, $Ca = 0.0079$, and $\beta = 30$ ($\epsilon = 7.06$); (d) 2:1 contraction with $k = 0.17$, $Ca = 0.011$, and $\beta = 20$ ($\epsilon = 4.55$). In all cases the location of sudden expansion or contraction is at $\zeta = 0$.
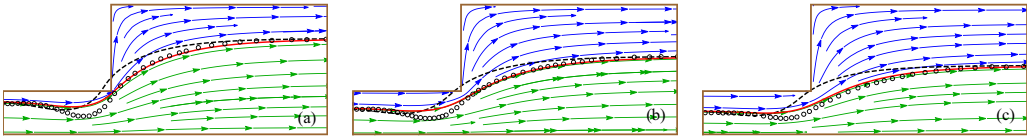
FIG. 5. Numerically computed interfacial profile (solid red line) in the upper half channel of the sudden 1:3 expansion with aspect ratio $\beta = 10$ together with the flow field of both phases (colored stream lines) for a fixed capillary number Ca = 0.0148 ($\epsilon = 1.48$), upon varying $k$. The experimental results (empty circles) and the long-wave approximation (dashed lines) are shown for comparison. (a) $k = 0.354$; (b) $k = 0.664$; (c) $k = 0.886$.

somewhat underestimates the amplitude of the upstream capillary ridge as compared to experiment. For example for $k = 0.354$ in Fig. 4(a), the minimal width of the thread in experiment reaches $\sim 60\%$ of its upstream width $\eta_{-\infty}$, while in the numerical solution it is $\sim 75\%$. Yet, the capillary instability does not seem to materialize in the 1:3 expansion and it may require a larger value of the expansion ratio $A$.

Notice that the interface determined using the long-wave theory (dashed lines), which does not explicitly account for the actual flow domain, in some cases crosses the channel boundary rendering the solution nonphysical. To illustrate this, we plot the numerical profiles (red solid line), the experimental data (symbols), and the approximate solution (dashed line) together with the (upper half) channel boundary for 1:3 expansion in Figs. 5(a)–5(c) upon varying $k$ for a fixed Ca $\approx 0.01$. The numerically computed flow field of both fluids is also shown (as colored stream lines). It can be readily seen that the approximate interface crosses the channel side walls at $x = 0$ in, e.g., Fig. 5(a). The numerical profiles computed with FEM, on the other hand, agree very well with the experimental result almost everywhere, except the near vicinity (upstream) of the expansion, where the numerical solution somewhat underestimates the amplitude of the capillary ridge [see, e.g., Fig. 5(a)]. The discrepancy is probably due to the fact that the interface approaches the channel corner at $x = 0$. The distance between the interface and the corner point for the sudden expansion in Fig. 5(a) is only $\sim 9.5\ \mu$m, which is about half of the channel height $b = 20\ \mu$m. Since depth-averaged Hele-Shaw equations do not hold in the $\mathcal{O}(b)$ vicinity of the side wall, one may expect a rather different pressure distribution (due to a higher pressure drop) and flow around the corner than the one computed numerically using the Hele-Shaw hydrodynamics. In agreement with this argument, the discrepancy between the numerical solution and the experimental measurements diminishes as $k$ increases, i.e., as the thread becomes narrower and the gap between the interface and the corner point increases [see Figs. 5(b) and 5(c)].

In the experiments the fluid inertia was negligible, as the flow should satisfy the condition $(b/w)\text{Re} \ll 1$, where the Reynolds number is defined as Re $= \rho u b / \mu$, with $u = b^2 |\nabla p|/\mu$ being a characteristic velocity of the flow in a Hele-Shaw cell [23]. For biphasic flow, the Reynolds number based on the (heavier) disperse phase 1 reads Re $= \rho u_1 b / \mu_1 = \rho(1 + k)q_1/\mu_1 w_-$. The flow rate of FC40 oil in the experiments in Fig. 5 varied between 120 and 150 $\mu$L/h; using density of the FC40 oil $\rho = 1.85$ g/mL and viscosity 4.2 mPa s, for $w_- = 200\ \mu$m we arrive at Re $\approx 0.12$–0.17 $\ll w_-/b = 10$, indicating that the effect of fluid inertia is negligibly small and it is not likely to be the reason for the observed discrepancy between the experimental observations and the numerical solution.

The corresponding comparison for 3:1 contraction is depicted in Fig. 6. Notice that the width of the gap between the free boundary and the corner point is about the channel height, 19.5 $\mu$m, also resulting in a discrepancy between the experimental profile and the numerical solution upstream, right before the contraction. Nevertheless, given that the solution of the full 3D low-capillary-number free boundary problem with ultrathin lubrication films is computationally expensive, the Hele-Shaw approximation yields a simple 2D formulation that can be efficiently solved on a standard PC yielding quite accurate predictions.
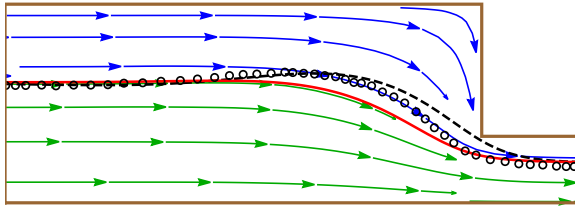
FIG. 6. Numerically computed interfacial profile (solid red line) in the upper half channel of the sudden 3:1 contraction with $\beta = 30$ for $k = 0.664$ and Ca $= 0.0079$ ($\epsilon = 7.06$); colored stream lines stand for the flow field of both fluids. The experimental results (empty circles) and the long-wave approximation (dashed lines) are shown for comparison.

## VI. CONCLUDING REMARKS

In the present paper we studied the stationary biphasic co-flow through a sudden change in a width (expansion or contraction) of Hele-Shaw channel. Using depth-averaged Hele-Shaw hydro-dynamics and neglecting transverse pressure variation (i.e., assuming gentle streamwise variance in the flow), it is possible to reduce the problem of determining the shape of the horizontal projection of the tip of the free interface separating the two fluids to a single third-order nonlinear ordinary differential equation. This equation can be readily integrated numerically subject to parallel co-flow conditions upstream and downstream from the expansion or contraction. Within the approximate model the shape of the interface depends on two dimensionless parameters: $k$, which incorporates the flow rate and viscosity ratios of the two fluids and expansion or contraction width ratio $A$. The other two parameters—the capillary number Ca, measuring the relative importance of the viscous and surface tension forces, and the Hele-Shaw aspect ratio $\beta$—only slightly affect the interfacial profiles by rescaling them in the streamwise direction by a factor $\epsilon^{\frac{1}{3}}$, where $\epsilon = \text{Ca}\beta^2$. Relaxing the assumption of gentle variation of the flow in the streamwise direction, we formulated and numerically solved (employing the finite element method), the corresponding 2D free-boundary problem using the approximate solution as the initial guess for the shape of the interface. The theoretical predictions show a fair agreement with our experimental results. However, the numerical solution somewhat underestimates the amplitude of the capillary ridge emerging prior to a sudden expansion or contraction, probably due to the proximity of the interface to the channel side wall where the Hele-Shaw description fails. It suggests that perhaps full 3D numerical simulations of the confined biphasic co-flow are required to clarify the observed discrepancy. In any case, our results indicate that the amplitude of the capillary ridge (for moderate expansion ratios up to 1:3) is not large enough to narrow and destabilize the confined stream of the disperse phase prior to the sudden expansion and cause its breakup.

## APPENDIX: NORMAL STRESS BOUNDARY CONDITION AT THE INTERFACE

The normal stress boundary condition at the interface separating the two fluids (see Fig. 1) is given by

$$\boldsymbol{n} \cdot (\boldsymbol{\sigma}_2 - \boldsymbol{\sigma}_1) \cdot \boldsymbol{n} = \gamma \nabla \cdot \boldsymbol{n}, \tag{A1}$$

where $\boldsymbol{\sigma}$ is the stress tensor, $\boldsymbol{n}$ is the unit normal to the interface (pointing into the continuous phase 2), and $\gamma$ is the constant surface tension. The stress tensor (using Cartesian tensor notation) is given by $\sigma_{ij} = -p\delta_{ij} + \tau_{ij}$, where $\delta_{ij}$ is the Kronecker delta and $\tau_{ij} = \mu(\partial_j u_i + \partial_i u_j)$ is the viscous stress tensor.

For stationary interface, whereas the flow does not possess a normal component at the boundary, one can safely neglect the viscous contribution to the normal stress, $\tau_{ij} n_i n_j \approx 0$. Therefore, the normal stress boundary condition (A1) reduces to the equilibrium-type equation, where the pressure jump across the interface is balanced by the capillary (Laplace) pressure proportional to the mean curvature $\nabla \cdot n$:

$$\Delta p \equiv p_1 - p_2 = \gamma \nabla \cdot \boldsymbol{n}. \tag{A2}$$

We next assume that the interface is given by $y = \mathcal{F}(x, z)$, where $z \in [-b/2, b/2]$. The mean curvature $\nabla \cdot \boldsymbol{n}$ of the stationary interface in the right-hand side of Eq. (A2) then can be written as

$$
\begin{aligned}
\nabla \cdot \boldsymbol{n} &= -\frac{\partial}{\partial x}\left[\frac{\mathcal{F}_x}{\left(1 + \mathcal{F}_x^2 + \mathcal{F}_z^2\right)^{1/2}}\right] - \frac{\partial}{\partial z}\left[\frac{\mathcal{F}_z}{\left(1 + \mathcal{F}_x^2 + \mathcal{F}_z^2\right)^{1/2}}\right] \\
&= -\frac{\left(1 + \mathcal{F}_z^2\right)\mathcal{F}_{xx} - 2\mathcal{F}_x\mathcal{F}_z\mathcal{F}_{xz} + \left(1 + \mathcal{F}_x^2\right)\mathcal{F}_{zz}}{\left(1 + \mathcal{F}_x^2 + \mathcal{F}_z^2\right)^{3/2}},
\end{aligned}
\tag{A3}
$$

where $\mathcal{F}_x$, $\mathcal{F}_z$, etc., stand for the corresponding partial derivatives of $\mathcal{F}$. Assuming that the interface shape can be written as $y = \mathcal{F}(x, z) = g(z) + f(x)$, where $f(x)$ is the projection of the tip of the interface onto the horizontal $(x, y)$ plane, we find that Eq. (A3) reduces to

$$\nabla \cdot \boldsymbol{n} = -\frac{(1 + g'^2)f'' + (1 + f'^2)g''}{(1 + g'^2 + f'^2)^{3/2}}, \tag{A4}$$

Now consider the coordinate system, obtained by rotation of the original coordinate system in the $(x, y)$ plane, in a way such that the at specific point $(x_0, y_0)$ at the interface the curve $f(x)$ is locally horizontal, i.e., meaning $f'(x_0) = 0$. Then $-f''(x_0) = 1/\mathcal{R}$, where $\mathcal{R}$ is the 2D radius of curvature of the interface in $(x, y)$ plane and thus Eq. (A2) without loss of generality for an arbitrary $z$ reduces to

$$\frac{\Delta p}{\gamma} = \frac{-g'' + (1 + g'^2)\mathcal{R}^{-1}}{(1 + g'^2)^{3/2}}. \tag{A5}$$

The shape of the interface should be determined by solving Eq. (A5) for some constant values of $\Delta p$ and $\mathcal{R}$. Thus for $\mathcal{R} \to \infty$ (e.g., far from the abrupt change of channel width at $x = 0$) Eq. (A5) reduces to

$$\frac{\Delta p}{\gamma} = -\frac{g''}{(1 + g'^2)^{3/2}}. \tag{A6}$$

Looking for an even convex solution (recall that the disperse phase does not wet the bounding walls at $z = \pm b/2$) satisfying $g(z) = g(-z)$ such that $g'(\pm b/2) = \mp\infty$ (i.e., $dz/dy = 0$ at the boundary $z = \pm b/2$) leads to the semicircular meniscus solution:

$$g(z) = \frac{\gamma}{\Delta p}\sqrt{1 - \left(\frac{\Delta p}{\gamma}\right)^2 z^2}, \quad \Delta p = \frac{2\gamma}{b}. \tag{A7}$$

The case of finite $\mathcal{R} \gg b$ can be handled similarly. We first rewrite the Eq. (A5) as

$$\frac{\mathcal{R}g''}{(-\alpha\sqrt{1 + g'^2})(1 + g'^2)} = 1,$$

where we introduced the dimensionless parameter $\alpha = \mathcal{R}\Delta p/\gamma$. Then for the last equation over $z$ we obtain

$$\mathcal{R}\tan^{-1}g' - \frac{\alpha\mathcal{R}}{\sqrt{-1+\alpha^2}}\left(\tan^{-1}\frac{g'}{\sqrt{1+g'^2}\sqrt{-1+\alpha^2}} + \tan^{-1}\frac{\alpha g'}{\sqrt{-1+\alpha^2}}\right) = z + C,$$

where $C$ is the constant of integration. Using the same boundary conditions at the bounding walls of the Hele-Shaw cell, i.e., $g'(\pm b/2) = \mp\infty$, gives the two relations

$$\frac{\mathcal{R}}{2}\left(-\pi + \pi\frac{\alpha}{\sqrt{-1+\alpha^2}} + \frac{2\alpha\cot^{-1}(-1+\alpha^2)}{\sqrt{-1+\alpha^2}}\right) = \frac{b}{2} + C,$$

$$\frac{\mathcal{R}}{2}\left(\pi - \pi\frac{\alpha}{\sqrt{-1+\alpha^2}} - \frac{2\alpha\cot^{-1}(-1+\alpha^2)}{\sqrt{-1+\alpha^2}}\right) = -\frac{b}{2} + C,$$

resulting in $C = 0$ and

$$\frac{b}{R} = -\pi + \pi\frac{\alpha}{\sqrt{-1+\alpha^2}} + \frac{2\alpha\cot^{-1}(-1+\alpha^2)}{\sqrt{-1+\alpha^2}}. \tag{A8}$$

Equation (A8) determines the pressure jump across the interface $\Delta p$ as a function of $\mathcal{R}$ and $b$. In the limit $\alpha \gg 1$ it admits the expansion in the series in powers of $\alpha^{-1}$ as

$$\frac{b}{\mathcal{R}} = \frac{2}{\alpha} + \frac{\pi}{2\alpha^2} + \frac{4}{3\alpha^3} + \mathcal{O}(\alpha^{-4}).$$

The last equation can be readily inverted to give

$$\alpha = \frac{2\mathcal{R}}{b} + \frac{\pi}{4} + \left(\frac{1}{3} - \frac{\pi^2}{32}\right)\frac{b}{\mathcal{R}} + \frac{\pi}{128}(-10 + \pi^2)\left(\frac{b}{\mathcal{R}}\right)^2 + \mathcal{O}\left(\frac{b^3}{\mathcal{R}^3}\right).$$

Substituting the definition of $\alpha = \mathcal{R}\Delta p/\gamma$ in the last equation and keeping only two leading terms gives

$$\Delta p \approx \gamma\left(\frac{2}{b} + \frac{\pi}{4\mathcal{R}}\right). \tag{A9}$$

The result in Eq. (A9) agrees with Eq. (6.1) in [17], where the more general analysis of a pressure jump across a *moving* interface displacing a viscous fluid is provided. Notice that in [17] there are also dynamic contributions to the pressure jump, e.g., $\mathcal{O}(\frac{\gamma}{b}\mathrm{Ca}_n^{2/3})$ at the leading order, where the capillary number $\mathrm{Ca}_n = U_n\mu_2/\gamma$ is based on the velocity of the interface displacement $U_n$. In our case of stationary interface we have $U_n = 0$, while the static contribution to the pressure jump due to finite in-plane curvature [the third term in the right-hand side of Eq. (6.1)] in [17] is identical to the one obtained here [the second term in the right-hand side of Eq. (A9)].

[1] H. S. H. Shaw, Investigation of the nature of surface resistance of water and of stream-line motion under certain experimental conditions, Trans. Inst. Nav. Archit., London **40**, 21 (1898).

[2] H. Lamb, *Hydrodynamics* (Dover Publications, New York, 1945).

[3] P. G. Saffman and G. I. Taylor, The penetration of a fluid into a porous medium or Hele-Shaw cell containing a more viscous liquid, Proc. R. Soc. London, Ser. A **245**, 312 (1958).

[4] G. Taylor and P. G. Saffman, A note on the motion of bubbles in a Hele-Shaw cell and porous medium, Q. J. Mechanics Appl. Math. **12**, 265 (1959).

[5] D. Bensimon, L. P. Kadanoff, S. Liang, B. I. Shraiman, and C. Tang, Viscous flows in two dimensions, Rev. Mod. Phys. **58**, 977 (1986).

[6] A. Huerre, O. Theodoly, A. M. Leshansky, M.-P. Valignat, I. Cantat, and M.-C. Jullien, Droplets in Microchannels: Dynamical Properties of the Lubrication Film, Phys. Rev. Lett. **115**, 064501 (2015).

[7] M. Nagel and F. Gallaire, Boundary elements method for microfluidic two-phase flows in shallow channels, Comput. Fluids **107**, 272 (2015).

[8] Y. Ling, J. M. Fullana, S. Popient, and C. Josserrand, Droplet migration in a Hele-Shaw cell: Effect of the lubrication film on the droplet dynamics, Phys. Fluids **28**, 062001 (2016).

[9] T. Beatus, R. H. Bar-Ziv, and T. Tlusty, The physics of 2D microfluidic droplet ensembles, Phys. Rep. **516**, 103 (2012).

[10] C. Priest, S. Herminghaus, and R. Seemann, Generation of monodisperse gel emulsions in a microfluidic device, Appl. Phys. Lett. **88**, 024106 (2006).

[11] F. Malloggi, N. Pannacci, R. Attia, F. Monti, H. Willaime, and P. Tabeling, Monodisperse colloids synthesized with nanofluidic technology, Langmuir **26**, 2369 (2010).

[12] Z. Li, A. M. Leshansky, S. Matais, L. M. Pismen, and P. Tabeling, Step-emulsification in a microfluidic device, Lab Chip **15**, 1023 (2015).

[13] X. Ge, B. Y. Rubinstein, Y. He, F. N. O. Bruce, L. Li, A. M. Leshansky, and Z. Li, Double emulsions with ultrathin shell by microfluidic step-emulsification, Lab Chip **21**, 1613 (2021).

[14] B. Shen, J. Ricouvier, F. Malloggi, and P. Tabeling, Designing colloidal molecules with microfluidics, Adv. Sci. **3**, 1600012 (2016).

[15] K. J. Humphry, A. Ajdari, A. Fernández-Nieves, H. A. Stone, and D. A. Weitz, Suppression of instabilities in multiphase flow by geometric confinement, Phys. Rev. E **79**, 056310 (2009).

[16] S. Afkhami and Y. Renardy, A volume-of-fluid formulation for the study of co-flowing fluids governed by the Hele-Shaw equations, Phys. Fluids **25**, 082001 (2013).

[17] C.-W. Park and G. M. Homsy, Two-phase displacement in Hele Shaw cells: Theory, J. Fluid Mech. **139**, 291 (1984).

[18] F. P. Bretherton, The motion of long bubbles in tubes, J. Fluid Mech. **10**, 166 (1961).

[19] L. E. Stillwagon and R. G. Larson, Fundamentals of topographic substrate leveling, J. Appl. Phys. **63**, 5251 (1988).

[20] S. Kalliadasis, C. Bielarz, and G. M. Homsy, Steady free-surface thin film flows over topography, Phys. Fluids **12**, 1889 (2000).

[21] R. D. Lenz and S. Kumar, Steady two-layer flow in a topographically patterned channel, Phys. Fluids **19**, 102103 (2007).

[22] Wolfram Research, Inc., Mathematica, Ver. 12.2 (Wolfram Research, Inc., Champaign, IL, 2020).

[23] G. K. Batchelor, *An Introduction to Fluid Dynamics* (Cambridge University Press, Cambridge, UK, 1967).

*Correction:* The affiliation indicators for the first, second, and fourth authors were misarranged and have been remedied.